

Diffusion of triplet excitons in an operational Organic Light Emitting Diode

M. Lebental¹, H. Choukri¹, S. Chénais¹, S. Forget¹, A. Siove¹, B. Geffroy², and E. Tutiš³

¹ CNRS, Université Paris Nord, UMR 7538, Laboratoire de Physique des Lasers, 93430 Villetaneuse, France

² CEA, Laboratoire de Physique des Interfaces et Couches Minces, Ecole Polytechnique, 91128 Palaiseau, France

³ Institute of Physics, P. O. Box 304, HR-10000 Zagreb, Croatia

(Dated: November 8, 2018)

Measurements of the diffusion length L for triplet excitons in small molecular-weight organic semiconductors are commonly carried out using a technique in which a phosphorescent-doped probe layer is set in the vicinity of a supposed exciton generation zone. However, analyses commonly used to retrieve L ignore microcavity effects that may induce a strong modulation of the emitted light as the position of the exciton probe is shifted. The present paper investigates in detail how this technique may be improved to obtain more accurate results for L . The example of 4,4'-bis(carbazol-9-yl)1,1'-biphenyl (CBP) is taken, for which a triplet diffusion length of $L=16 \pm 4$ nm (at 3 mA/cm²) is inferred from experiments. The influence of triplet-triplet annihilation, responsible for an apparent decrease of L at high current densities, is theoretically investigated, as well as the 'invasiveness' of the thin probe layer on the exciton distribution. The interplay of microcavity effects and direct recombinations is demonstrated experimentally with the archetypal trilayer structure [N,N'-bis(naphthalen-1-yl)-N,N'-bis(phenyl)]-4,4'-diaminobiphenyl (NPB)/CBP/2,9-dimethyl-4,7-diphenyl-1,10-phenanthroline (named bathocuproine, BCP). It is shown that in this device holes do cross the NPB/CBP junction, without the assistance of electrons and despite the high energetic barrier imposed by the shift between the HOMO levels. The use of the variable-thickness doped layer technique in this case is then discussed. Finally, some guidelines are given for improving the measure of the diffusion length of triplet excitons in operational OLEDs, applicable to virtually any small molecular-weight material.

PACS numbers: 71.20.Rv, 71.20.Nr, 71.35.Cc

I. INTRODUCTION

The performance of organic light emitting diodes (OLED) has been pushed towards the ultimate limit of 100 % internal quantum efficiency thanks to the use of phosphorescent guest-host systems [1, 2]. In phosphorescent organic light-emitting devices, triplet exciton diffusion plays a major role: it has been recently reported that one can take advantage of it to efficiently monitor energy transport from the exciton creation zone up to the emissive dopants to allow fine color tuning [3, 4]. Exciton diffusion also plays a key role in bilayer photovoltaic organic devices as it governs the exciton dissociation efficiency [5, 6].

In these cases, the interesting characteristic of triplet excitons is their long diffusion length compared to singlet excitons. Indeed, the diffusive properties of triplet and singlet excitons are substantially different. While the typical singlet exciton diffusion lengths are in the range of a few nanometers in amorphous organic semiconductors [7], a question arises about the order of magnitude for triplet excitons. The diffusion length in a steady-state and linear regime is usually described by $L_0 = \sqrt{D\tau}$, D being the diffusion coefficient and τ the exciton lifetime. On one hand, the lifetime of triplet states (from μ s to ms range) is much higher than typical singlet states lifetime (ns). Meanwhile, it is not so straightforward to compare the relative orders of magnitude of D for singlets and triplets, since the physical mechanisms behind their diffusion are fairly different. Exciton migration between two non-emissive triplet states (e.g. host molecules in host-

guest phosphorescent systems) is a pure Dexter mechanism, consisting in a simultaneous exchange of electrons in the LUMO and holes in the HOMO levels. In contrast, energy transfer between two singlets can be accounted both by a Dexter mechanism or a Forster non-radiative dipole-dipole coupling even if the latter usually predominates [8, 9]. As a consequence, D coefficients could tend to be lower for triplet excitons than for singlet excitons [10].

It turns out to be an irrelevant task to seek an universal order of magnitude for triplet exciton diffusion lengths, which are expected to be highly dependant on the nature of the material, its degree of purity, the nature and strength of the excitation, etc. This difficulty is experimentally confirmed: measured triplet diffusion lengths cover a range going from a few nanometers in phosphorescent dendrimers [11] to several microns in pure organic crystals [12]. Furthermore, even for a well-known material such as CBP, the reported diffusion lengths are highly scattered [13, 14, 15, 16].

It is then of foremost importance to develop both theoretical and experimental tools to improve our understanding of triplet exciton dynamics. Triplet migration has been a topic of intense research firstly in organic crystals [12] and aromatic hydrocarbons [17] and then more recently in amorphous organic semiconductors [18, 19, 20]. Along with theoretical work, it is essential to have reliable direct measurements of diffusion lengths to support both theory and device design. The aim of the present paper is to identify the main physical processes and parameters that have to be taken into account to perform

a meaningful measurement of triplet exciton diffusion in an operational device, and to propose some guidelines for extracting these parameters experimentally.

The paper is organized as follows: In Section II, we present an experimental measurement of the triplet diffusion length in CBP based on the technique first proposed by Baldo et al. [21]. To enhance the reliability of the measurement, we used a device specially designed to exclude two physical effects likely to mask the diffusion process, namely *microcavity effects* and *bulk carrier recombinations*. Indeed, the optical field variation related to microcavity effects is huge in this case (the technique requires thick diodes), even if its influence is usually neglected in comparable devices [3], leading to questionable values for the diffusion lengths. These experimental results serve as a basis for a discussion of the relevant key points in the following sections. Section III is a theoretical investigation which aims at precisely defining the exciton diffusion length, gives the analytical solution for the steady-state exciton distribution in presence of triplet-triplet annihilation, and proposes a quantitative criterium to quantify the strength of this bi-particle process. The influence of the thin sensing layer is also investigated, motivated by an insight that its presence may considerably alter the distribution of triplets in the device. In Section IV, we use an archetypal diode structure [3, 16] to experimentally illustrate the combined influence of bulk carrier recombinations and optical field variations. For the same device we also demonstrate the poor hole-blocking efficiency of a hetero-junction usually considered as a strong barrier for holes and therefore as the exciton generation zone [3, 15]. We conclude by the comparison of our result for the triplet diffusion length in CBP to the values published by other authors. The concluding section lists our recommendations for a reliable measurement of triplet diffusion lengths.

II. DIFFUSION MEASUREMENT

A. Choice of the technique

Two types of methods have been commonly used to measure the diffusion length of triplet excitons and both have been applied to CBP: excitons are created either by optical excitation or by carrier recombination in an operational OLED device. The techniques based on optical excitation enable easy time-resolved studies, while those based on electrical excitation provide a higher control of the exciton formation zone and are closer to the operating conditions of real devices. With optical techniques (photocurrent spectroscopy [13, 22] or time-resolved spectral decay analysis [14]), obtaining a clear signature of diffusion is intricate when the absorption length of the laser (of the order of 50 nm [14]) has the same order of magnitude as the diffusion length, which is the case in practice. This issue disappears under electrical excitation, where localized "sheets" of

excitons are achievable. In fact the strong localization of the exciton formation is a very robust consequence of the energy barrier and the carrier accumulation at the heterojunction in multilayer OLEDs. The spatial scale of the exciton formation zone is then of the order of the thickness of a few molecular monolayers, reflecting the space distribution of blocked carriers. This is much less than one is likely to get under most favorable circumstances from the space charge effects caused by the low carrier mobility, as illustrated in Ref. [23]. Thus in general, exciton formation zones are highly localized at hetero-junctions [15, 16, 24]. Furthermore all quenching processes are included, like exciton-exciton or exciton-polaron annihilation, which may be desirable when one attempts to obtain an effective diffusion length directly exploitable to build real light-emitting devices. In the technique used by D'Andrade et al. [16], excitons are created at one edge of a thick CBP layer doped with Iridium(III) tris(2-phenyl-pyridinato-N,C^{2'}) (Ir(ppy)₃), and the light emitted by the phosphor is collected for various thicknesses of the doped layer. A diffusion length of 8.3 ± 1 nm was then derived for CBP. Zhou et al. [15] pointed out that these measurements yielded information about an Ir(ppy)₃-doped CBP system rather than about a pure undoped CBP layer. They proposed a refined model to extract the diffusion length in pure CBP from the same set of data and obtained about 60 nm. However, in their fitting procedure two unknown parameters have to be extracted simultaneously (namely the diffusion constants for the doped and the undoped region) under the assumption that all excitons are created at the interface between the Hole Transporting Layer (HTL) and the Emitting Layer (EML) (in this case between NPB and CBP). As shown in Sec. IV B, this assumption is rather questionable for this particular heterojunction.

In the present paper, we use the technique described by Baldo et al. [21] in which excitons are generated at a heterojunction, diffuse in a neat undoped region until they reach a thin phosphorescent layer acting as a probe. Since only short-range (~ 1 nm) Dexter transfer is possible from host to host or from host to guest in the case of triplets, the emissive layer truly acts as a local probe for triplet excitons, with a spatial resolution almost only limited by the thickness of the sensing layer.

B. Choice of parameters

The choice of CBP in this study is motivated by the fact that it has been the subject of many investigations, leading to several measurements of the triplet exciton diffusion length, with different techniques and highly scattered experimental results.

The OLED structure and the HOMO/LUMO levels of the different materials are shown in Fig. 1. It is made up of a standard layer stack embedding the CBP ma-

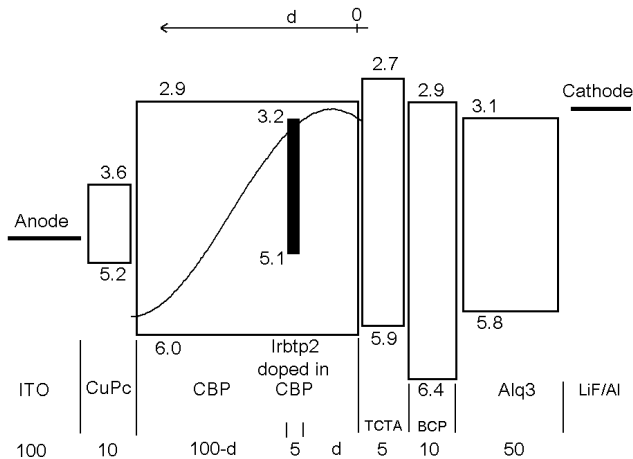


FIG. 1: Structure of the diode used in Sec. II. The layer thicknesses are indicated on the bottom in nanometers. The HOMO and LUMO energy levels are taken from literature [25, 26] and specified for each compound (negative values). The profile of the optical field is plotted in the CBP layer (see Sec. IV A for details).

trix: indium tin oxide (ITO) anode coupled to a copper phthalocyanine (CuPc) layer for hole injection (HIL), aluminium tris(8-quinolinolato)(Alq₃) layer for electron transport (ETL) and LiF/Al cathode for electron injection. In order to efficiently block both electrons and holes and generate excitons in the form of a localized "sheet", two additional layers were used, each of them being well-known to efficiently block one type of carriers: 4,4',4"-tris(carbazol-9-yl)-triphenylamine (TCTA) for electrons and BCP for holes. The triplet exciton sensor (the emitting layer EML) is a 5-nm-thick layer of CBP doped with 6 % Iridium(III) bis[2-(2'-benzothienyl)-pyridinato-N,C3'] acetylacetonate (Ir(btp)₂ acac) and inserted at a position defined by the d parameter equal to the distance between the CBP/TCTA interface and the center of the sensing layer (see Fig. 1). The choice of Ir(btp)₂ was motivated by its phosphorescent efficiency [27, 28] and its emission spectrum easily resolved from those of the other compounds used in this OLED [29] (see on Fig. 2). The thicknesses of the different layers are given in Fig. 1. The CBP layer is noticeably thick because relatively long diffusion lengths are expected. Moreover the Alq₃ and CBP layers are optimized so that the generation zone of excitons is located at a position where the optical field corresponding to the red emission of the phosphorescent layer is as flat as possible over a long distance. If this condition is not met, the variation of the optical field should be carefully taken into account and it may be difficult to decouple it from the effect of diffusion, as further discussed in Sec. IV where details about the calculation of the optical field are also given. On the relevant scale (i.e. d between 0 and 40 nm), its variation appears to be less than 20 % and could hardly be reduced. The thickness

of the EML has been set to 5 nm. This is thin enough to limit the influence of its position d on the optical field. A theoretical investigation of the role of the sensing layer in electronic properties and exciton transport will be exposed in Sec. III.

When evaporating the thin sensing layer, the question may arise of how the doping rate and the layer thickness can be accurately controlled and reproduced [15]. We solved this issue by systematically making four devices in each single run: two of them corresponding to a "reference diode" (fixed d parameter), and the other two to some other value of d . The electroluminescence was then always normalized to the reference diode.

The glass substrate covered by ITO was cleaned by sonication and prepared by a UV-ozone treatment. The layers were then deposited by sublimation under high vacuum (10^{-6} - 10^{-7} mbar) at a rate of 0.1-0.2 nm/s in a thermal evaporator. An *in situ* quartz crystal was used to monitor the thickness of the layer depositions with a precision of 5 %. The organic materials and the LiF/Al cathode were deposited in a one-step process without breaking the vacuum.

After deposition, all the measurements were performed at room temperature and under ambient atmosphere, without any encapsulation. For each diode with a specific position d of the thin Ir(btp)₂:CBP layer, the current-voltage-luminance characteristics and electroluminescence spectra (in the direction normal to the substrate) were collected and recorded with a PR 650 SpectraScan spectrophotometer for different currents from 0 to 50 mA, corresponding to a current density $J=0$ -166 mA/cm².

C. Results

The Current-Voltage (I-V) curves appear in Fig. 3. The high voltage threshold (about 20 V) is consistent with the unusually large thicknesses of our devices compared to those commonly reported in the literature. It may be noticed that the I-V characteristics are similar whatever the position d of the sensing layer, showing its negligible influence on the transport properties.

The external quantum efficiency is maximum for a current density around 3 mA/cm² with a value of 3.2 ± 0.5 % for $d = 7.5$ nm (see insert of Fig. 3), and we observed a roll-off of the external quantum efficiency with the current, which is a classical feature of phosphorescence-based OLEDs usually attributed to triplet-triplet quenching between guest molecules [24, 30].

The typical electroluminescence spectrum shown in Fig. 4 comprises two different contributions. The red structured peak is the clear signature of Ir(btp)₂ (see Fig. 2), but the blue peak (centered at 450 nm) cannot be associated with any photoluminescence (PL) spectrum. Furthermore, the optical field variations do not allow explaining such a difference between the observed

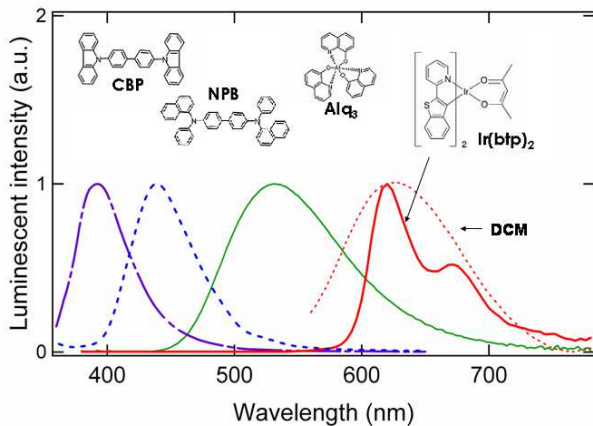


FIG. 2: Photoluminescent spectra of some of the compounds used in this paper with their chemical structure. The electroluminescent spectrum of DCM is plotted in dotted line.

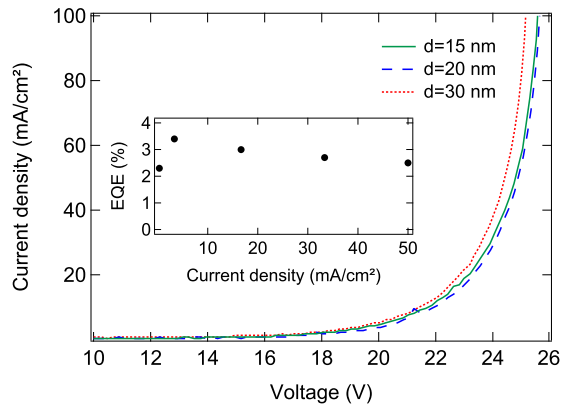


FIG. 3: Current density versus voltage curves for diodes with different d positions of the probe layer. Inset: External quantum efficiency (EQE) versus current density for a diode with $d=7.5$ nm.

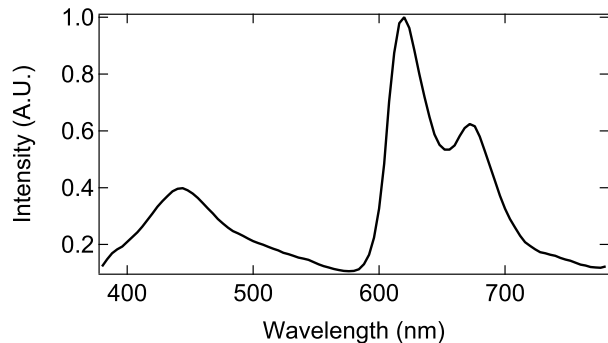


FIG. 4: Electroluminescent spectrum for a diode described in Fig. 1 with $d=12.5$ nm at a current density of 3.3 mA/cm².

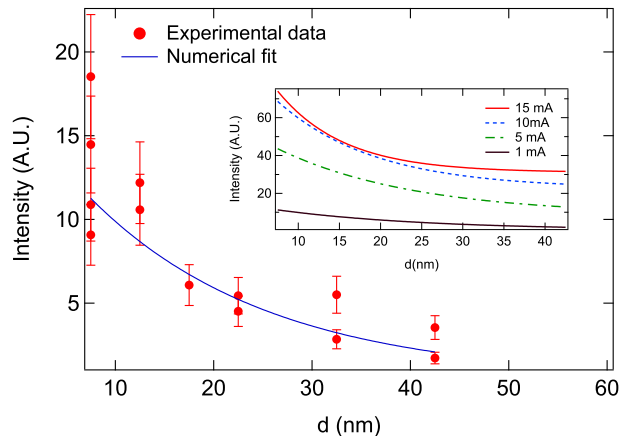


FIG. 5: The circles correspond to the red detected intensity corrected by the optical field versus the d position of the probe layer at $J = 3.3$ mA/cm². The fit by Eq. (1) is plotted in continuous line. Inset: Fits from Eq. (1) of experimental data for different current densities.

electroluminescence spectrum and any of the PL spectra. We then conclude that this blue peak originates from exciplexes [31] formed at the TCTA/BCP interface, which is consistent with the large energy shifts between their LUMO (0.4 eV) and HOMO levels (0.5 eV) [32, 33] and with a clear spectral redshift with respect to the TCTA PL spectrum (maximum around 410 nm) [34] [50].

For distances d long enough for singlet exciton density to vanish (typically less than 10 nm [7]), the red emission from Ir(btp)₂ may have several origins: it may result from direct recombinations between holes and electrons traveling in bulk CBP (the electrons would have crossed the thin TCTA layer by tunneling or any other process); it may also come from triplet excitons diffusing from the CBP/TCTA interface. The mechanism leading to triplet excitons being formed in CBP from exciplexes is beyond the scope of this paper and deserves further investigation since many processes can be invoked. Whatever the mechanism at work, the net result is a triplet exciton population in a restricted area around the CBP/TCTA heterojunction, which can not come back to the TCTA layer due to its larger energy gap.

The intensity emitted by the phosphorescent material for a given current density $J=3.3$ mA/cm² is integrated over its spectral range and then plotted versus d in Fig. 5 after dividing by the amplitude of the optical field at the same position. A downward trend from the interface ($d=0$) is clearly visible, which evidences a diffusion process, since direct recombinations should yield a signal which is independent of d (after compensation of the optical field variations). When the current is increased, the probe intensity shows a kind of "plateau" for large d values, which can be attributed to direct recombin-

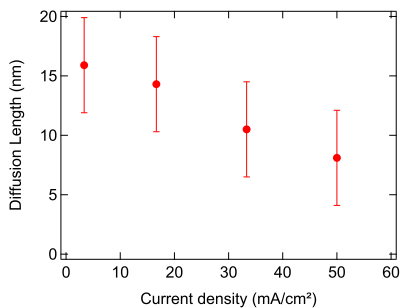


FIG. 6: Effective diffusion length L of triplet exciton versus the current density, defined from Eq. (1) and inferred from the fits shown in the insert of Fig. 5.

tions and indicates that more and more electrons pass through the thin TCTA layer. The experimental data can consequently be fitted by the following expression:

$$I(d, J) = [A(J) + B(J) e^{-d/L(J)}] \times E_{opt}(d) \quad (1)$$

where $I(d, J)$ is the intensity of light emitted for a position d of the sensing layer at a given current density J , and $E_{opt}(d)$ is the optical field. Here, we fit the data with a constant (A) and a simple exponential decay ($B e^{-d/L}$), which is much simpler than the refined analysis presented in Sec. III. However it still gives the typical distance L (called hereafter "effective diffusion length of triplet excitons") over which excitons can diffuse, even if the non-linear contribution of the triplet-triplet annihilation does not allow, strictly speaking, to consider an exponential (or bi-exponential) behavior. The constant term A stands for direct recombinations so that B/A corresponds to the ratio of light intensity generated from triplet excitons over light intensity generated from direct recombinations. A , B and L depend *a priori* on the current density J .

The fits using Eq. (1) and presented in insert of Fig. 5 show that the number of direct recombinations grows with the current density as expected. From the fits, the effective diffusion length of triplet excitons is estimated to be 16 ± 4 nm at low currents, and turns out to decrease down to 8 nm when the current increases (see Fig. 6) as expected due to bimolecular interactions such as triplet-triplet annihilations or triplet-polaron quenching [10, 24, 30].

This effective diffusion length, even at low current densities, is small compared to what could be expected from the high lifetime of CBP triplet excitons (14 ± 8 ms [14]). Moreover it is lower than previously reported values under electrical excitation: 46 ± 3 nm at 10 mA/cm² by Sun et al. [3] and 60 nm at unspecified current density by Zhou et al. [15]. However we discuss in Sec. IV how direct recombinations, microcavity effects and barrier energetics may invalidate some aspects of these measurements.

In order to unambiguously attribute the down-

ward tendency to triplet exciton diffusion, a control experiment was carried out with a fluorescent compound, 4-(dicyanomethylene)-2-methyl-6-(p-dimethylaminostyryl)-4H-pyran (DCM), instead of the phosphorescent Ir(btp)₂. Actually DCM triplet states do not emit light and CBP triplet excitons cannot transfer their energy towards singlet states of DCM as Dexter transfer requires total spin conservation [51]. Therefore the comparison between both devices allows a clear distinction between triplet diffusion and direct recombinations. Moreover the DCM and Ir(btp)₂ emission spectra exhibit a similar envelope (see Fig. 2) so that the optical field effect is not modified. The only difference with respect to previous experiments is the lower doping rate of DCM in the CBP matrix (1.5 % in weight), necessary to limit concentration quenching [52]. As a result, OLEDs were realized with the DCM-doped CBP thin layer set at two d positions characterized by an optical field having almost identical values ($d=12.5$ nm and $d=42.5$ nm), and which are both far enough from the recombination zone to neglect the influence of singlet exciton diffusion. The measured DCM emitted intensity is 15 % smaller at $d=12.5$ nm than at $d=42.5$ nm ($J = 3.3$ mA/cm²) which is compatible with the measurement uncertainties and evidences direct recombinations in bulk CBP. In the case of the Ir(btp)₂:CBP doped layer, the difference between the intensity emitted at these two positions is much larger (5 times more red light at $d=12.5$ nm than at $d=42.5$ nm), which is then an unambiguous signature of triplet exciton diffusion.

Moreover, with the DCM:CBP layer, we clearly observed that the color emitted by the diode shifted from the sky-blue emission of dominant exciplexes at low currents to magenta as the current was increased, which is an additional proof that the "plateau" observed above (corresponding to the $A(J)$ parameter in Eq. (1)) is the manifestation of current-dependent direct recombinations.

The strategy developed in this Section to obtain an estimation of the diffusion length, albeit specific to CBP, can be applied to virtually any material. It is the objective of the following Sections to discuss in more detail the physical parameters influencing the measurement of triplet exciton diffusion lengths. We need first to examine, from a theoretical point of view, how the intensity emitted by the probe relates to the actual exciton density, especially when triplet-triplet annihilation is present or/and when the probe layer itself affects the exciton motion.

III. DIFFUSION LENGTH

In the limit of low exciton concentration, their distribution in space $n(x)$ goes exponentially with x , the distance from the source, with a scale set by the intrinsic diffusion length of triplet excitons L_0 . However, the distribution in space is not expected to be the same in the case when the triplet-triplet quenching activates, as the strength of the source of excitons increases. Additionally, if a probe used

for detecting triplet excitons is efficient in their trapping and recombining, it may considerably disturb their distribution in space. These effects are analyzed below starting from the usual diffusion-decay model. The dependence of the signal on the distance from the source is derived when one or both effects are present. It is concluded that the invasiveness of the probe does not present a serious obstacle in extracting the proper value of L_0 from the experiment. Conversely, the effect of triplet-triplet quenching at higher source intensity, if not analyzed properly, may lead to significant underestimate of L_0 .

A. Fundamental equation

The equation that governs the diffusion of triplet excitons in an organic one-dimensional [53] layer is

$$\frac{\partial n}{\partial t} = D \frac{\partial^2 n}{\partial x^2} - \gamma_T n - \gamma_{TT} n^2 \quad (2)$$

The right hand side of this equation is made up of three different contributions. First the term $D \frac{\partial^2 n}{\partial x^2}$ characterizes the genuine diffusion of triplet excitons through the D diffusion coefficient, which is assumed to be isotropic and constant through the whole CBP layer. Then, the term $\gamma_T n$ gathers all the processes responsible for a decreasing of the triplet exciton density, where only one triplet exciton is involved in. It is made up of the radiative and non-radiative desexcitations γn , the singlet-triplet annihilation $\gamma_{ST} n_S n$, the polaron-triplet annihilation $\gamma_{PT} n_P n$ [30], and eventually of other quenching processes. For the sake of simplicity, we assume an uniform value of γ_T , which is probable since the densities of singlet excitons and polarons become roughly constant (or even negligible) in a bulk material a few nanometers away from the generation zone of excitons. Finally the term $\gamma_{TT} n^2$ corresponds to the triplet-triplet annihilation which was observed under typical OLED operation conditions [24, 30]. Its influence will be evaluated below. For fitting with experiments presented in Sec. II, we focus on the stationary state solution of equation,

$$D \frac{\partial^2 n}{\partial x^2} - \gamma_T n - \gamma_{TT} n^2 = 0, \quad (3)$$

in the presence of a steady source at $x = 0$. The solution $n(x)$ is sought in the portion of the space $x > 0$, away from the source. The strength of the source, G , sets the value of the exciton current at the $x = 0$ boundary, $G = -Dn'(0)$.

Obviously, the relative importance of the two decay terms in Eq. (3) depends on the concentration of excitons, with their influence being comparable at the n_0 characteristic density: $n_0 \equiv \gamma_T/\gamma_{TT}$. In the limit of the rare exciton gas, $n \ll n_0$, the distribution of triplet excitons is given by the simple exponential dependence, $n(x) \propto \exp(-x/L_0)$, set by the only intrinsic length scale

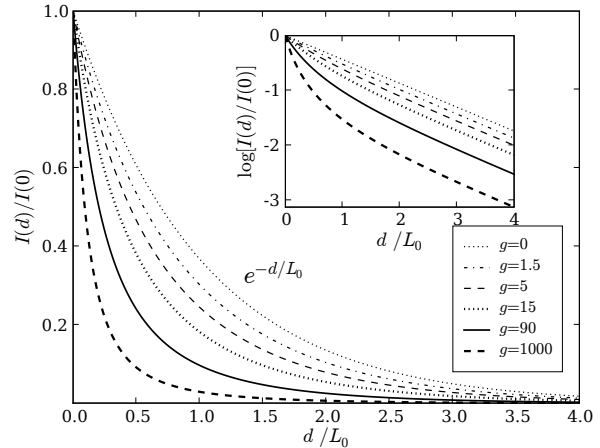


FIG. 7: The calculated dependence of the emitted signal in the presence of triplet-triplet quenching and non-invasive probe inferred from Eq. 8. The insert gives the semi-logarithmic view of the same set of data.

in the equation, the *triplet diffusion length*,

$$L_0 \equiv \sqrt{\frac{D}{\gamma_T}}. \quad (4)$$

B. Triplet-triplet quenching

The spatial dependence $n(x)$ complicates as the strength of the source G increases, and when the only dimensionless parameter of the problem,

$$g \equiv \frac{G \gamma_{TT}}{L_0 \gamma_T^2}, \quad (5)$$

rises above unity [54]. The nonlinear differential equation Eq. (3) for the steady state has to be solved in that case, and the details are given in Appendix A. The solution may be written in the form

$$n(x) = \frac{3 n_0}{2 \left(\sinh \frac{x+d_{TT}}{2L_0} \right)^2}, \quad (6)$$

where a new length scale d_{TT} is introduced, $d_{TT}/L_0 = \ln(1/\mu)$, with the parameter μ related to the dimensionless source strength g through

$$g = \frac{6(1+\mu)\mu}{(1-\mu)^3}. \quad (7)$$

The parameter μ approaches zero for a weak source $g \ll 1$, and approaches unity for a strong source, $g \gg 1$. A strong source implies $d_{TT} \ll L_0$, with $n(x)$ falling much faster than $\exp(-x/L_0)$ in the region $0 < x < L_0$.

The profile of $n(x)/n(0)$ determines the variation of the emitted light in the limit of a non-invasive and infinitely thin probe layer at the d position,

$$\frac{I(d)}{I(0)} = \frac{\left(\sinh \frac{d_{TT}}{2L_0}\right)^2}{\left(\sinh \frac{d+d_{TT}}{2L_0}\right)^2}. \quad (8)$$

Examples of this dependence for various values of the g parameter are shown in Fig. 7. The figure shows that the spatial decay rate effectively increases as the strength of the exciton source increases, in accordance with our experimental findings. However, as the variation of intensity with d is no more exponential when the influence of triplet-triplet quenching grows, the concept of "effective diffusion length", largely used in the literature as well as in Sec. II is, strictly speaking, an ill-defined parameter. In ideal cases, the data should enable by a proper fit the extraction of L_0 and d_{TT} , from which it should be possible to derive γ_{TT} . In our case however, there are several obstacles against extracting the value of the triplet-triplet quenching parameter γ_{TT} from the experimental data. First, less scattered experimental data may be required for precise evaluation of the parameter g determining the shape of the curves in Fig. 7. More importantly, in order to determine γ_{TT} from g one still has to know other parameters in Eq. (5), most notably the strength of the exciton source G , and calculating its absolute value is not straightforward.

However, it is informative to have an idea of the order of magnitude that should be expected for g in real cases. For that purpose, we can consider that a given ratio η of injected carriers are converted into potentially diffusing triplet excitons. Then at low current density, η would reach the maximum value of 0.75 if neither exciplex would be involved in, nor other lossy intermediate states. The strength of the exciton source G can thus be written $G \simeq \eta J/q$, where q is the elementary charge. The other parameters needed to compute g are taken from [14] ($\tau_T = 1/\gamma_T = 15$ ms and $\gamma_{TT} \simeq 1.10^{-14}$ cm³/s), and our experimental value of L_0 is considered ($L_0 \sim 15$ nm). Then for $J \simeq 1$ mA/cm² and $\eta = 0.75$, g is about 1000. Whatever the realistic value of η , g is probably higher than 1 [55]. The triplet-triplet annihilation is then supposed to have a strong influence on measurements even at low current densities, which may be the explanation of such small effective diffusion lengths reported in electrically-driven structures.

C. Influence of the sensing layer

The detection of the exciton diffusion by the probe technique used in Sec. II assumes that the sensing layer at different position d does not influence the conditions of exciton generation, diffusion and recombination. The 'invasiveness' of the sensing layer is, however, not fully avoidable in practice. Two aspects of the invasiveness

are imaginable. One aspect is related to the trapping of charge carriers in the sensing layer, whereas the other relates to the trapping of excitons.

The change of the electric field distribution caused by trapped charges [35] is not expected to affect very much the motion of excitons which are neutral objects. On the other hand it may be noted that, for a given external voltage, the difference in the spatial profile of the electric field in two devices with different position d of the sensing layer implies different charge distribution among interfaces, with a probable effect on exciton generation and recombination. In our case however, as shown in Fig. 3, this effect was negligible. In a more general fashion, it can be ignored as soon as the devices are compared for the same value of the current running through them.

If the effects of charge trapping do not seem relevant in the experiments of Sec. II, the consequences of exciton trapping must be considered more carefully. Actually a sensing layer of thickness $\delta = 5$ nm is introduced to absorb a fraction of the triplet excitons and convert them into photons. Ideally, this layer is thin and absorbs only a small fraction of triplets, without significantly perturbing their distribution in space. In practice, this implies rather small signal from the probe, which may then be masked by the light emission from exciton recombinations elsewhere in the device. Realistically, the doping of the order of a few percents made through several monolayers of the host material, may already represent rather invasive probe. Actually the separation between doped molecules is of the order of few molecular sizes, and then also of the order of the Dexter radius, the scale involved in the diffusion of triplet excitons. The sensing layer then disturbs the genuine dependence $n(x)$, implicating a deviation from the ideal case. This effect may be easily modeled by replacing the decay term $-\gamma_T n$ by as stronger one $-\gamma_{SL} n$, with $\gamma_{SL} > \gamma_T$ within the sensing layer $d < x < d + \delta$. The measured quantity is then the number of excitons absorbed by the sensing layer per unit time, proportional to

$$I(d) = \int_d^{d+\delta} \gamma_{SL} n(x) dx. \quad (9)$$

For the sake of simplicity, the effect of the invasiveness of the sensing layer is first examined in the limit of low exciton density, when the triplet-triplet quenching term may be neglected, but in fact it does not modify strongly these results (the full problem including triplet-triplet quenching is exposed in Appendix C). The linear differential equation is then treated straightforwardly (see Appendix B), and the profile $n(x)$ as well as the dependence $I(d)$ may be calculated for any value of the source strength. It is found that the result $I(d)/I(0)$ depends on the parameter β_I which measures the 'invasiveness' of the probe and combines the thickness of the sensing layer δ and its absorption coefficient γ_{SL} , as

$$\beta_I = \frac{1 - \kappa^2/\kappa_{SL}^2}{1 + (\kappa/\kappa_{SL}) \coth \kappa_{SL} \delta}. \quad (10)$$

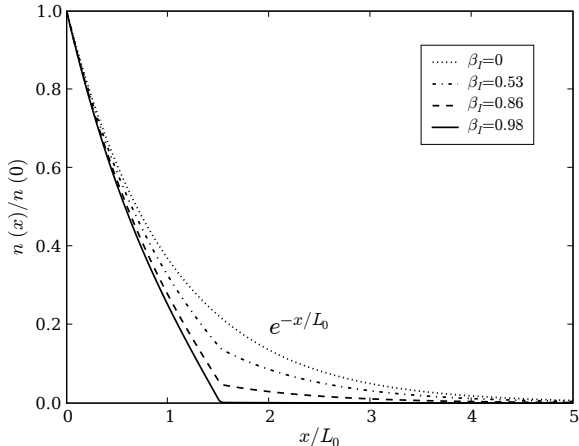


FIG. 8: The influence of the probe on the distribution of excitons in space $n(x)/n(0)$ for various levels of invasiveness β_I . The sensing layer of thickness $\delta = 0.05 L_0$ is placed as $d = 1.5 L_0$.

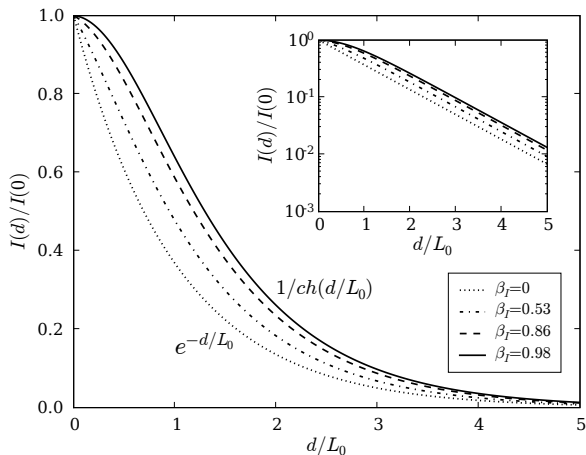


FIG. 9: The dependence of the signal intensity $I(d)/I(0)$ on the position d of the probe, for various levels of its invasiveness β_I . The formulae are indicated on the graph for the limits of non-invasive and strongly invasive probe.

Here κ and κ_S stand, respectively, for $\kappa \equiv (\gamma_T/D)^{1/2} = L_0^{-1}$ and $\kappa_{SL} \equiv (\gamma_{SL}/D)^{1/2}$. The result for $I(d)$ reads as

$$\frac{I(d)}{I(0)} = \frac{1}{\cosh(d/L_0) + (1 - \beta_I) \sinh(d/L_0)}, \quad (11)$$

with the limits of $\exp(-d/L_0)$ and $1/\cosh(d/L_0)$, respectively for the case of non-invasive ($\beta_I \rightarrow 0$), and strongly invasive probe ($\beta_I \rightarrow 1$). Fig. 8 shows that a thin layer efficient in exciton trapping and recombination considerably affects the shape of $n(x)$, the distribution of excitons in space. Related effect on the dependence of the signal $I(d)$ on the distance from the source,

described through Eq. (11), is shown in Fig. 9. Even for strongly invasive probe, the effect shows mostly for $d < L_0$, while the dependence $I(d) \propto \exp(-d/L_0)$ is restored at bigger distances.

In Sec. II, the value of the diffusion length was inferred from the experimental data without taking into account the invasiveness of the sensing layer. According to the analysis proposed in this part, the "real" diffusion length should then be about 15-30 % shorter than what plotted in Fig. 6.

IV. BULK CARRIER RECOMBINATIONS AND MICROCAVITY EFFECTS

In thick diodes, more precisely when the active layer has a thickness comparable or higher than $\lambda/4n$ (n being the refractive index and λ the wavelength in vacuum), the amplitude of the optical field is modulated at the scale of the diode and thus the assumption that the intensity emitted by the probe layer only reflects the exciton density at a given point is not generally valid. As shown in Eq. (1), this microcavity effect happens as a modulation of the light emitted by the probe layer. Although it also modulates the exciton diffusion pattern, its influence is especially important for direct carrier recombinations, since the latter occur with equal probability across the whole thickness of the material under investigation. This has been illustrated in Sec. II and is discussed in more detail hereafter with a NPB/CBP/BCP trilayer structure, commonly used in previous reports on exciton diffusion measurements [3, 15]. The occurrence of direct carrier recombinations is linked to the NPB/CBP junction, which properties are discussed in the second part of this section.

A. Microcavity effects

Usual OLED devices are intrinsically weak microcavities, formed on one side by a highly reflecting metallic cathode, and on the other side by the ITO/Glass interface. As a consequence, there is a stationary wave pattern inside the OLED, leading to a modulation of the optical field. The probability to observe emission from a molecule (either fluorescent or phosphorescent) depends on the density of optical modes and on the effective mode volume at the location of the molecule. The influence of the optical field modulation has then to be taken into account to correctly describe the OLED light emission. If this effect is not predominant in most classical OLEDs because each layer thickness is only a few tens of nanometers wide, it is clearly not the case in structures used for diffusion length measurements where very thick layers are used [3, 16]. For instance, for the green emitter and the structure used in [3], the optical field is minimum approximately in the middle of the layer and reaches a maximum near the edges. Since expected diffusion patterns (expo-

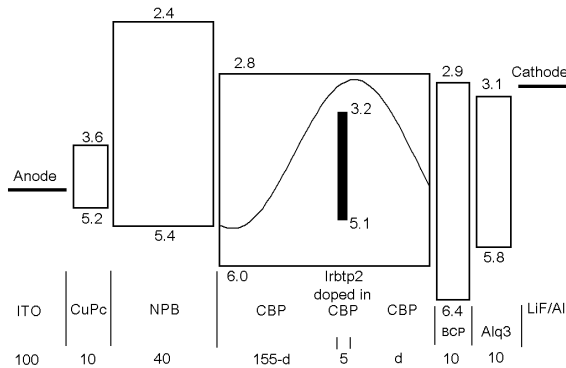


FIG. 10: Structure of the diode used in Sec. IV A. The layer thicknesses are indicated on the bottom in nanometers. The HOMO and LUMO are taken from literature [25, 26] and specified for each compound (negative values). The profile of the optical field is plotted in the CBP layer.

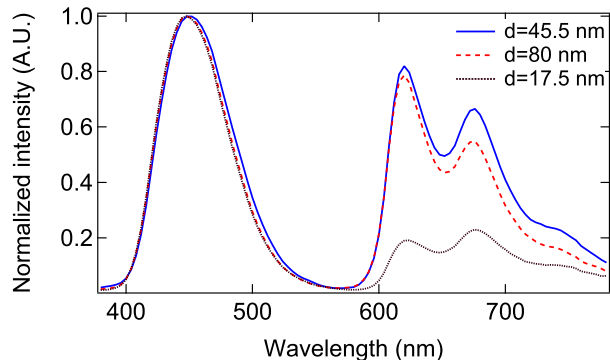


FIG. 11: Electroluminescent spectra of diodes described in Fig. 10 for different d positions at $J=3.3$ mA/cm².

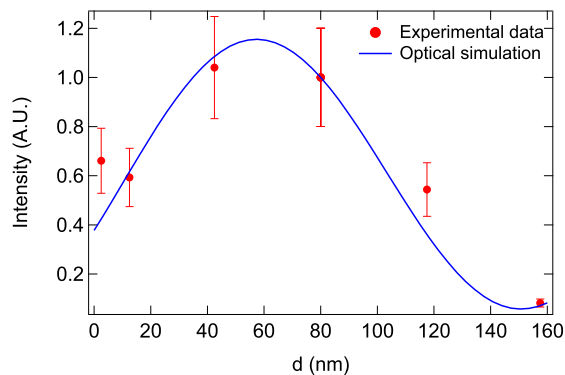


FIG. 12: The circles correspond to the red detected intensity normalized to its blue part versus the d position of the probe layer at $J = 3.3$ mA/cm². The profile of the optical field calculated over the spectral range of Ir(btp)₂ emission is plotted in continuous line.

ponential decays from both edges) as well as optical field variations appear to go in the same direction, it is likely that the extraction of the only diffusion effects in such a structure is problematic. To keep away from this difficulty, we investigated a similar structure in which the green emitter was replaced by a red one, in such a way that the optical field was clearly distinguishable from a diffusion signature, i.e. maximum in the middle of the CBP layer (see Fig. 10).

In order to calculate this emission probability, we assume that every single molecule is an independent emitter creating its own interference pattern. The planar geometry of the diode can be considered as a Fabry-Perot type microcavity, characterized by a strong dependence of the output light on both wavelength and polarization [36, 37, 38]. We here only consider the light emitted at normal incidence, which is obviously not dependent on polarization. The calculations were carried out using the ETFOS software (Fluxim Inc.) which is based on the numerical method described in [39] and takes into account the wavelength-dependence of the complex indices of all materials involved in the full multilayer device. The model yields the normalized intensity collected in the far-field as a function of wavelength and position d of the sensing layer.

The structure of the diodes is presented in Fig. 10. The diodes have been realized using the experimental procedure described in Sec. II. The spectra presented in Fig. 11 show two contributions: one broad blue peak due to NPB (see the comparison with photoluminescent spectra in Fig. 2), and the characteristic structured spectrum of Ir(btp)₂. In Fig. 12, the red emission (integrated over the spectral range of the phosphorescent emission), plotted against d , is normalized with respect to the magnitude of the blue NPB peak, to account for possible fluctuations of the total luminance from one evaporation batch to another. A nice agreement is noticed between the experimental data and the profile of the optical field obtained from simulations [56]. The only adjusted parameter here is the vertical scale.

This behavior could result from direct electron-holes recombinations on the phosphorescent molecules or, alternatively, from the diffusion of triplet excitons formed at the NPB/CBP and CBP/BCP interfaces over a very large distance (>160 nm) so that the light emission would eventually follow the shape of the optical field. To discriminate between these two effects, we performed the same experiment with DCM, a fluorescent compound, and we observed that the measured red light versus the position d agreed also very well with the optical field (not shown here). As the DCM molecule could not emit light from its triplet state and as singlet excitons can not diffuse so far, the red light necessarily comes from recombinations of carriers flowing in opposite directions in the bulk. This suggests that the observed Ir(btp)₂ emission results from direct exciton formation on these phosphorescent guests, which is consistent with the hole trapping property of Ir phosphors [35]. Furthermore this observa-

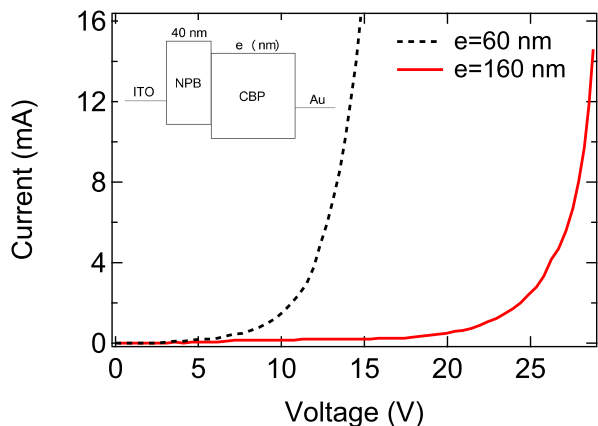


FIG. 13: Current density versus voltage curves for hole-only diodes with different thicknesses of the CBP layer. Insert: structure of the hole-only diodes.

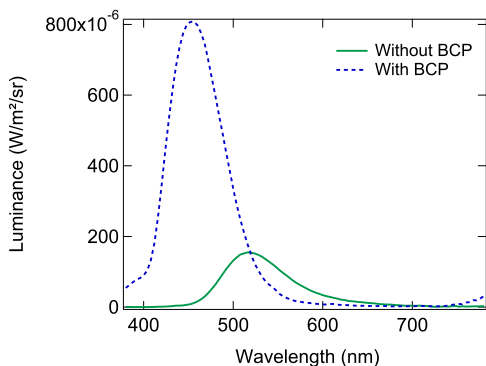


FIG. 14: Electroluminescent spectra of diodes NPB/CBP/Alq₃ (continuous line) and NPB/CBP/BCP/Alq₃ (dotted line) at $J=1.7$ mA/cm².

tion implies that a non-negligible amount of holes passes through the NPB/CBP interface.

The example described in this Section provides a clear illustration of a situation where microcavity effects dominate so much that no diffusion length can be straightforwardly extracted from experimental data. Although one may try to numerically factor-out the contribution of the optical field from the experimental results, the dominance of the microcavity effects implies that the uncertainties, both on the experimental data and those related to the optical field simulations (layer thicknesses, refractive indices, etc.) reflect in the large uncertainties for the diffusion length.

B. Hole leakage through the NPB/CBP interface

In the experiment described just above, the evidence of direct recombinations in CBP also implies that holes

do cross the NPB/CBP interface. Here the heterojunction does not truly act as a blocking interface for both types of carriers, and diffusion of excitons is not the main channel of exciton generation in the sensing layer. This feature has to be examined with some attention as it is in contradiction with both basic energetic considerations and some previous reports [3, 15].

Indeed, the NPB/CBP interface is usually described as an efficient hole blocking barrier [40] due to the high energetic shift in the HOMO levels of the two compounds [25]: the HOMO level of NPB is higher than the HOMO level of CBP [24] by 0.5 eV [41] to 0.8 eV [42]. However it is known that vacuum levels may not be necessarily aligned at hetero-junctions, resulting in an interface dipole. Although the interface dipole for NPB/CBP has not been measured directly to the best of our knowledge, the interface dipole in the case of organic-organic hetero-junctions is determined by the difference in the charge neutrality levels [43], which have been measured independently and turn out to be identical and equal to 4.2 eV [43]. As a result, vacuum level alignment seems to be a valid assumption in this case.

Yet, the experiments in Sec. IV A show that holes cross the barrier, which is not expected given that the energetic jump (0.5 to 0.8 eV) is 20 to 30 times higher than thermal energy at operating temperatures. According to OLED electrical models which consider hetero-junctions, such as the MOLED code [44, 45], the hopping probability through such a high energetic barrier is very unlikely, even when the effects of energy disorder are taken into account [46, 47, 48]. It can be asked whether electrons accumulated at the interface can help in some way the leakage of holes. For instance, exciplexes could be suspected to play the role of intermediate states conveying holes from NPB to CBP.

To answer that question, electrons were removed by performing "hole-only" experiments. Bilayer diodes have been fabricated, consisting of NPB and CBP deposited between an ITO anode and a gold cathode (see insert in Fig. 13). The conditions of deposition were similar to those described in Sec. II, but the gold layer was only 20 nm thick and the rate of deposition was less than 0.1 nm/s to limit the likelihood of short-circuits which often appear with a gold cathode due to the penetration of metallic particles into the organic layers. The I-V curves for two different CBP layer thicknesses (60 and 160 nm respectively ; the NPB layer is kept equal to 40 nm) are presented in Fig. 13. They show a clear diode behavior with a voltage threshold having the same order of magnitude as the diodes described in Sec. II. In addition, it can be seen that for a given current (ie. for a given electric field in each material) the voltage drop across the whole 200-nm thick device is approximately two times the voltage drop across the 100-nm thick device, at least well above threshold. Since the two organic materials have comparable dielectric constants, this probably indicates that the electric field is merely constant throughout the device and then that the charge accumulated at the junc-

tion is not significant (in contrast, a good hole-blocking interface would yield a voltage drop ratio given by the ratio of the CBP thicknesses, here ~ 2.7). This evidences a hole flow through the NPB/CBP interface in spite of the large difference between their HOMO levels, without the assistance of electrons. Actually if electrons would have been injected in the device, they would have been detected through the blue emission of the NPB or CBP layer. However, some diffusion of gold particles into the organic materials cannot be completely ruled out, so that percolation paths could be created for holes.

Another way to evidence that holes cross without the assistance of electrons is to look at some exciton emission at the junction, which is expected to come from NPB here since its gap is lower than the CBP one. Indeed, from the electroluminescence spectra in Fig. 14 of the NPB/CBP/BCP/Alq₃ diodes studied in Sec. IV A, we observed a blue peak assigned to NPB, whereas, when the BCP layer was removed [57], this NPB emission vanished while the distinctive green emission spectrum of Alq₃ became clearly visible. In this latter case, as the absence of NPB emission cannot be attributed to microcavity effects, it confirms that very few holes accumulate at the NPB/CBP interface, while most of them travel up to the Alq₃ layer where they recombine with electrons. This process cannot appear in the presence of the BCP layer, since the CBP/BCP hetero-junction is a well-established hole blocking interface, which is confirmed here. The appearance of NPB emission in presence of BCP could be attributed to a reduced electric field in CBP (resulting from the hole accumulation at the CBP/BCP interface) which would make a little uneasy the hole crossing from NPB to CBP.

This configuration is interesting since it almost corresponds to a standard structure, studied by D'Andrade et al. [16], and re-examined in more detail by Zhou et al. [15], in which a thick Ir(ppy)₃-doped CBP layer was inserted between NPB and pure CBP in order to infer the triplet exciton diffusion length of CBP. In these works, all the excitons were assumed to be created at the interface between NPB and Ir(ppy)₃-doped CBP and subsequently diffuse in CBP [15]. We believe that the efficiency saturation observed when increasing the width of the doped layer in these devices cannot be attributed to the single diffusion of CBP triplet excitons, even perturbed, or shortened by the presence of the dopant. Firstly it could be argued that given the energy gaps, as shown by the previous experiment, excitons are formed rather in NPB, which might transfer their energy to the phosphors via a Forster energy transfer in virtue of a good spectral overlap. But since holes have the potential to easily cross the barrier (as we have shown), it can be thought that some excitons are formed directly on the phosphor, and then the generation zone of excitons could be as large as a few nanometers, which matches the value of 8 nm reported in [16] for the exciton diffusion length. Another important aspect that should be considered is the opportunity for a Ir(ppy)₃ exciton to diffuse directly to another guest site

[10, 49].

Through the lens of these experiments, it consequently appears that the diffusion lengths obtained under the assumption of the NPB/CBP hetero-junction being a highly efficient hole blocking barrier [3, 15, 16] are questionable, and that a deeper insight into this interface is needed to fully understand the corresponding results.

V. CONCLUSION

In this work, we presented a thorough analysis of triplet exciton diffusion length measurements by the repositionable thin sensing layer technique in operational OLED devices. We demonstrated the importance of a well-defined thin exciton generation zone to avoid charge carriers flowing along the diode and thus leading to direct recombinations in the probe layer. Through careful design of the diode structure, we also circumvented masking effects of optical field variations. As a result, a 16 ± 4 nm effective diffusion length for triplet excitons in CBP was inferred from experimental data in a working electroluminescent device. Comprehensive study of the different processes at stake in such a structure allows extraction of some useful guidelines for measuring triplet exciton diffusion lengths in other materials:

1. An ideal case would be to create excitons only at the heterojunction between the material of interest and a higher-gap semiconductor, in order to avoid excitons being formed preferentially in the latter. This is in practice challenging since triplet host materials (especially for green or blue phosphors) would be themselves high-bandgap materials. This was the case in the illustrated example CBP here, which thus required the design of a special structure.
2. In real cases, direct recombinations occur, with a variable magnitude according to the injected current. Away from the generation zone of excitons, the emission pattern resulting from direct trapping of electrons and holes in the repositionable thin sensing layer reproduce the shape of the optical field inside the diode. The relative importance of direct recombinations and diffusion can be straightforwardly measured by replacing the phosphorescent dopant by a fluorescent one. In all cases, the optical field modulates both the diffusion and direct recombination pattern, and has to be carefully taken into account.
3. Triplet-triplet annihilation can be significant even at moderate current densities and causes an apparent decrease of the measured diffusion length. When the goal is to design a device where e.g. color control is governed by exciton diffusion, it is important to measure it at realistic current densities. If

data with low scattering are obtained, it is theoretically predicted that the decay will not be a single exponential decay any more.

4. The choice of the probe layer (thickness and doping rate) should be thought of as a trade-off between the intensity of light that can be detected from low-exciton density regions, and its invasiveness, as discussed in Section III C.

Acknowledgments

The authors are grateful to D. Tondelier and D. Adès for experimental and technological support and to E. Bogomolny and M.-C. Castex for fruitful discussions. M. L. acknowledges the C'nano Ile-de-France program for financial support. This work was supported in part by Croatian MSES grant No. 035-0352826-2847.

APPENDIX A: TRIPLET-TRIPLET QUENCHING

In terms of rescaled, dimensionless quantities, $z = x/L_0$ and $y(z) = n(x)/n_0$, the nonlinear equation acquires the form

$$y'' - y - y^2 = 0. \quad (\text{A1})$$

Multiplying this equation by $2y'$, the integration gives

$$y'^2 - y^2 - \frac{2}{3}y^3 = C, \quad (\text{A2})$$

C being a constant. The equation is rewritten as (note the sign used in taking the root),

$$\frac{dy}{\sqrt{y^2 + \frac{2}{3}y^3 + C}} = -dz. \quad (\text{A3})$$

In the case of *non-invasive* probe, and very wide diffusion layer, the requirement $n(x \rightarrow \infty) = 0$ sets $C = 0$. The integral on the left hand side may then be expressed in terms of hyperbolic functions. The dependence $y(z)$ (i.e. $n(x)$) is then easily obtained and follows to Eq. (6).

APPENDIX B: SEMI-INVASIVE PROBE LAYER

Given the form of the differential equation for $n(x)$ (see Eq. (3)) in the case without the triplet-triplet quenching, the solution is sought in the form:

$$\begin{aligned} Ae^{-\kappa x} + Be^{\kappa x} & \text{ for } 0 < x < d \\ Ce^{-\kappa_{SL}x} + Ee^{\kappa_{SL}x} & \text{ for } d < x < d + \delta \\ Fe^{-\kappa x} & \text{ for } d + \delta < x \end{aligned}$$

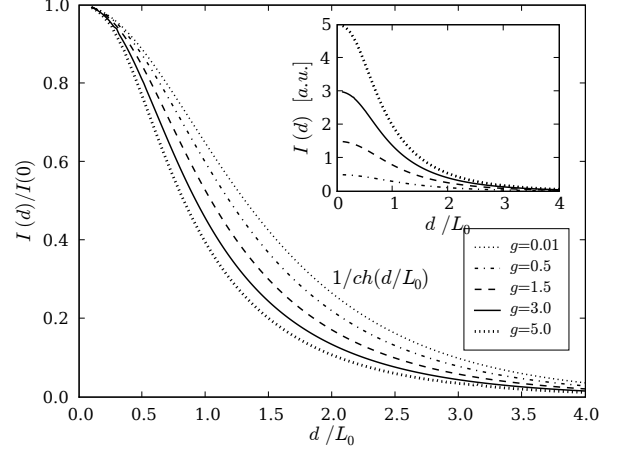


FIG. 15: The dependence of the strength of the signal $I(d)/I(0)$ on the position d of the probe for various strengths g of the triplet source (or triplet-triplet quenching rate). The insert shows the graphs un-normalized by the strength $I(0)$ of the signal.

Both $n(x)$ and its derivative should be continuous at junction points, $x = d$ and $x = d + \delta$. Those requirements set the four relations among coefficients A , B , C , E and F . These, together with the value of the strength G of the source of excitons at $x = 0$, $G = -Dn'(0) = D\kappa(A - B)$, determine the values of all the coefficients, A to F . The calculation is somewhat tedious if done manually, but straightforward if using some of the usual software tools for symbolic computation. The limiting case of strong invasiveness is particularly easy to treat.

APPENDIX C: INVASIVE PROBE LAYER AND TRIPLET-TRIPLET QUENCHING

The nonlinear differential equation that poses in the presence of triplet-triplet quenching may also be exactly solved in the presence of infinitely invasive probe (i.e. the forcing $n(d) = 0$). Then the integration constant C is directly related to the strength of the signal $I(d) = -Dn'(d) \propto \sqrt{C}$ via Eq. (A2). Similarly, the strength of the source at $x = 0$, $G = -Dn'(0)$, in dimensionless quantities, is given by

$$g = \sqrt{y_0^2 + \frac{2}{3}y_0^3 + C}, \quad (\text{C1})$$

where $y_0 \equiv y(0)$. This is one of the equations to be used in order to determine C and y_0 , while the second one is obtained by integrating Eq. (A3),

$$\int_0^{y_0} \frac{dy}{\sqrt{y^2 + \frac{2}{3}y^3 + C}} = - \int_{d/L_0}^0 dz = \frac{d}{L_0}. \quad (\text{C2})$$

This integral may be expressed in terms of the elliptic integral of the first kind $F(\psi|\alpha)$. From equations (C1) and (C2), the values y_0 and C for a given value g and d/L_0 are calculated numerically (as well as the value of the integral or related function $F(\psi|\alpha)$). The desired quantity $I(d)/I(0)$ is then obtained from

$$\frac{I(d)}{I(0)} = \frac{I(d)}{G} = \frac{\sqrt{C}}{\sqrt{y_0^2 + \frac{2}{3}y_0^3 + C}} \leq 1. \quad (\text{C3})$$

These results cannot be expressed in terms of elementary functions and the curves are directly plotted in Fig. 15.

As in the case without triplet-triplet quenching, the invasiveness of the sensing layer is affecting the dependence of the signal at small distances, in the same region where the triplet-triplet quenching effect is strongest, and for strong exciton source, the dependence at $d < L_0$ is again much steeper than $\exp(-d/L_0)$. The exponential behavior determined by L_0 re-establishes at distances further than L_0 . The insert in Fig. 15 shows the dependence of un-normalized signal for different strengths of the source.

-
- [1] M. A. Baldo, D. F. O'Brien, Y. You, A. Shoustikov, S. Sibley, M. E. Thompson, and S. R. Forrest, *Nature (London)*, **395**, 151 (1998).
- [2] B. W. D'Andrade and S.R. Forrest, *Advanced Materials*, **16**, 1585 (2004).
- [3] Y. Sun, N. C. Giebink, H. Kanno, B. Ma, M. E. Thompson, and S. R. Forrest, *Nature* **440**, 908 (2006).
- [4] Y. Sun and S.R. Forrest, *Appl. Phys. Lett.* **91**, 263503 (2007).
- [5] P. Peumans, A. Yakimov, and S.R. Forrest, *Journal of Applied Physics*, **93**, 3693 (2003).
- [6] Y. Shao and Y. Yang, *Adv. Mat.* **17**, 2841 (2005).
- [7] H. Choukri, A. Fisher, S. Forget, S. Chénais, M.-C. Castex, D. Adès, A. Siove, and B. Geffroy, *Appl. Phys. Lett.* **89**, 183513 (2006).
- [8] T. Forster, *Discuss. Faraday Soc.* **27**, 7 (1959).
- [9] R. C. Powell and Z. G. Soos, *Journal of Luminescence* **11**, 1 (1975).
- [10] M. A. Baldo and S. R. Forrest, *Phys. Rev. B* **62**, 10958 (2000).
- [11] E. Namdas, A. Ruseckas, I. D. W. Samuel, S.-C. Lo, and P. L. Burn, *Appl. Phys. Lett.* **86**, 091104 (2005).
- [12] V. Ern, P. Avakian, and E. Merrifield, *Physical Review* **148**, 862 (1966).
- [13] N. Matsusue, S. Ikame, Y. Suzuki, H. Naito, *Journal of Applied Physics* **97**, 123512 (2005).
- [14] N. C. Giebink, Y. Sun, and S.R. Forrest, *Organic Electronics* **7**, 375 (2006).
- [15] Y. C. Zhou, L. L. Ma, J. Zhou, X. M. Ding, and X. Y. Hou, *Phys. Rev. B* **75**, 132202 (2007).
- [16] B. W. D'Andrade, M. E. Thompson, and S. R. Forrest, *Advanced Materials* **14**, 147 (2002).
- [17] L. V. Levshin, G. A. Ketsle and Yu. A. Soinikov, *Journal of Applied Spectroscopy*, **45**, 584 (1986).
- [18] C. Rothe and A. Monkman, *Phys. Rev. B* **68**, 075208 (2003).
- [19] L. Sudha Devi, M. Al-Suti, C. Dosche, M.S. Khan, R. Friend, and A. Köhler, *Phys. Rev. B* **78**, 045210 (2008).
- [20] I. Fishshuk, A. Kadashchuk, L. Sudha Devi, P. Heremans, H. Bäessler, and A. Köhler, *Phys. Rev. B* **78**, 045211 (2008).
- [21] M. A. Baldo, D. F. O'Brien, M. E. Thompson, and S. R. Forrest, *Phys. Rev. B* **60**, 14422 (1999).
- [22] C. L. Yang, Z. K. Tang, W. K. Ge, J. N. Wang, Z. L. Zhang, X. Y. Jian, *Appl. Phys. Lett.* **83**, 1737 (2003).
- [23] E. Tutiš, D. Berner, and L. Zuppiroli, *J. Appl. Phys* **93**, 4594 (2003).
- [24] M. A. Baldo, C. Adachi, and S. R. Forrest, *Phys. Rev. B* **62**, 10967 (2000).
- [25] I. G. Hill and A. Kahn, *Journal of Applied Physics* **86**, 4515 (1999).
- [26] M. Ikai, S. Tokito, Y. Sakamoto, T. Suzuki, and Y. Taga, *Appl. Phys. Lett.* **79**, 156 (2001).
- [27] T. Tsuboi and N. Aljaroudi, *Journal of Luminescence* **119**, 127 (2006).
- [28] C. Adachi, M. A. Baldo, S. R. Forrest, S. Lamansky, M. E. Thompson, and R. C. Kwong, *Appl. Phys. Lett.* **78**, 1622 (2001).
- [29] S. Lamansky, P. Djurovich, D. Murphy, F. Abdel-Razzaq, H.-E. Lee, C. Adachi, P. E. Burrows, S. R. Forrest, and M. E. Thompson, *Journal of the American Chemical Society*, **123**, 4304 (2001).
- [30] S. Reineke, K. Walzer, and K. Leo, *Phys. Rev. B* **75**, 125328 (2007).
- [31] A. Weller, in M. Gordon and W. R. Ware (Eds), *Academic Press, London* (1975).
- [32] M. Cocchi, D. Virgili, G. Giro, V. Fattori, P. di Marco, J. Kalinowski, and Y. Shirota, *Appl. Phys. Lett.* **80**, 2401 (2002).
- [33] G. Li, C. H. Kim, Z. Zhou, J. Shinar, K. Okumoto, and Y. Shirota, *Appl. Phys. Lett.* **88**, 253505 (2006).
- [34] Y. Shirota, M. Kinoshita, and K. Okumoto, *Proc. SPIE-Int. Soc. Opt. Eng.*, **203**, 4464 (2002).
- [35] I. H. Campbell and B. K. Crone, *Appl. Phys. Lett.* **89**, 172108 (2006).
- [36] F. Jean, J.-Y. Mulot, B. Geffroy, C. Denis, and P. Cambron, *Appl. Phys. Lett.* **81**, 1717 (2002).
- [37] J. M. Leger, S. A. Carter, B. Ruhstaller, H.-G. Nothofer, U. Scherf, H. Tillman, and H.-H. Hörhold, *Phys. Rev. B* **68**, 054209 (2003).
- [38] H. Benisty, H. de Neve, and C. Weisbuch, *IEEE Journal of Quantum Electronics*, **34**, 1612 (1998).
- [39] B. Ruhstaller, T. Beierlein, H. Riel, S. Karg, J. C. Scott, and W. Riess, *IEEE J. Sel. Top. Quantum Electron.*, **9**, 723 (2003).
- [40] Y. Kim, B. Moon, and C.-S. Ha, *Journal of Applied Physics*, **100**, 064511 (2006).
- [41] H. Yang, W. Xie, Y. Zhao, J. Hou, and S. Liu, *Solid-State Electronics* **51**, 111 (2007).
- [42] C.-H. Cheng, Z.-Q. Fan, S.-K. Yu, W.-H. Jiang, X. Wanga, G.-T. Du, Y.-C. Chang, and C.-Y. Ma, *Appl. Phys. Lett.* **88**, 213505 (2006).

- [43] H. Vazquez, W. Gao, F. Flores, and A. Kahn, Phys. Rev. B **71**, 041306(R) (2005).
- [44] E. Tutiš, M. N. Bussac, B. Masenelli, M. Carrard, and L. Zuppiroli, J. Appl. Phys. **89**, 430 (2001).
- [45] H. Houili, E. Tutiš, H. Ltjens, M. N. Bussac, and L. Zuppiroli, Comput. Phys. Commun. **156**, 108 (2003).
- [46] J. Staudigel, M. Stössel, F. Steuber, and J. Simmerer, J. Appl. Phys. **86**, 3895 (1999).
- [47] H. Houili, E. Tutiš, I. Batistić, and L. Zuppiroli, J. Appl. Phys. **100**, 033702 (2006).
- [48] H. Houili, E. Tutiš, and L. Zuppiroli, Synthetic Metals **156**, 1256 (2006).
- [49] J. C. Ribierre, A. Ruseckas, K. Knights, S. Staton, N. Cumpstey, P. Burn, and I. Samuel, Phys. Rev. Lett. **100**, 017402 (2008).
- [50] A rough estimate of the exciplex energy, notwithstanding the exciplex binding energy and energetic disorder, is given by the difference between the TCTA HOMO level (-5.9 eV) and the BCP LUMO level (-2.9 eV) and corresponds to a wavelength of about 410 nm.
- [51] Triplet-to-singlet transfer might be possible if the donor exciton breaks up and reforms on the acceptor via incoherent electron exchange. However, as pointed out by Baldo et al. [21], this has to be considered as very unlikely since the energy required for dissociation, i.e. the exciton binding energy, approaches 1 eV in most systems.
- [52] The emitted intensity from DCM and Ir(btp)₂ can not be directly compared to each other due to their different quantum yields and concentration.
- [53] In Sec. II, the triplet excitons diffuse from the CBP/TCTA hetero-junction (plane $x = 0$) with a G constant rate and a uniform distribution in the y and z directions. This three-dimensional (3D) problem can thus be solved as an one-dimensional problem thanks to the planar geometry of the source term, but the parameters such as the diffusion length and the diffusion coefficient are still the same (ie. defined in 3D). In this configuration, the diffusion length is the same in the real three-dimensional system or in its reduction along the x axis. Thus we will only consider the latter case.
- [54] The quenching among triplet excitons in host is expected when they come close in terms of the Dexter radius, and similarly the quenching of triplet excitons and holes (polarons). This is since otherwise it is difficult to make the spin-flip required for triplet excitons to decay. This implies γ_{TT} and γ_{PT} being of the same order of magnitude. Therefore frequency of two processes is essentially given by the ratio of the concentrations of triplets and polarons $\gamma_{TP}n_P n_T / \gamma_{TT}n_T^2 \sim n_P/n_T$. For typical values of current density, mobility, electric field, and molecular size ($\mu_p \sim 10^{-4} \text{ cm}^2/\text{Vs}$, $F \sim 1 \text{ MV/cm}$, $J \sim 100 \text{ mA/cm}^2$, $a \sim 0.6 \text{ nm}$) the concentration of polarons is of the order of $n_P \sim 10^{-7}$ per molecule, while the creation rate of excitons/exciplexes at the heterojunction, for the same set of parameters, is estimated to $\nu \sim 10^3 \text{ s}^{-1}$ per molecular cross section. The density of triplets n_T is obtained upon considering the fraction α of excitons created being triplets, considering their diffusion over length L_0 , as well as accounting for their decay rate γ_T . For $\gamma_T \sim 10^6 \text{ s}^{-1}$ and $L_0 \sim 50 a$, the concentration of triplets per molecule turn to be $n_T \sim \alpha \times 10^{-4}$. This gives a plenty of room for the possibility that $n_T \gg n_P$, corresponding to the situation where triplet-triplet quenching is much more frequent than the quenching of triplets on polarons.
- [55] A rough estimation of $\eta \sim 10^{-2}$ can be inferred from the red part of the experimental spectra (see Sec. II), assuming 20 % efficiency in extracting photons and an isotropic emission over the upper half-plane. For $J=1 \text{ mA/cm}^2$, this implies $g \sim 10$.
- [56] The only small disagreement around $d = 0$ can be explained by excitons diffusing from the CBP/BCP interface as expected.
- [57] The thickness of the CBP layer was then 10 nm increased to minimize the changes in the optical field.